Article type : Research Article

Cardiac radioablation for atrial fibrillation: target motion characterization and treatment delivery considerations

Short running title: CR for AF: motion characterization

Suzanne Lydiard[1,2], Beau Pontré[3], Boris S Lowe[4], Helen Ball[1], Giuseppe Sasso[3,5,6], and Paul Keall[1]

[1] ACRF Image X Institute, University of Sydney, Sydney, Australia

[2]Ingham Institute for Applied Medical Research, Sydney, Australia

[3] Department of Anatomy and Medical Imaging, University of Auckland, Auckland, New Zealand

[4] Green Lane Cardiovascular Service, Auckland City Hospital, Auckland, New Zealand

[5] Cancer & Blood, Radiation Oncology, Auckland City Hospital, Auckland, New Zealand

[6]Department of Oncology, University of Auckland, Auckland, New Zealand

Corresponding Author: Suzanne Lydiard

E-mail: slyd6788@uni.sydney.edu.au

ABSTRACT

Purpose: The safe delivery of cardiac radioablation (CR) for atrial fibrillation (AF) is challenged by multi-direction target motion, cardiac rate variability, target proximity to critical structures, and the importance of complete target dose coverage for therapeutic benefit. Careful selection of appropriate treatment procedures is therefore essential. This work characterizes AF cardiac radioablation target motion and target proximity to surrounding structures in both healthy and AF participants to guide optimal treatment technique and technology choice.

Methods: Ten healthy participants and five participants with AF underwent MRI acquisition. Multi-slice, cardiac-gated, breath-hold cines were acquired and interpolated to create 3D images for 18-30 cardiac phases. Treatment targets at the left and right pulmonary vein ostia (CTV_{Left} and CTV_{Right} respectively) and adjacent cardiac structures were contoured and their displacements throughout the cardiac cycle were assessed. Target proximity to surrounding structures were measured. Free-breathing real-time 2D cine images were also acquired at 4 Hz frequency for between one- and two-minute duration. The motion of easily identifiable points within the target, diaphragm and sternum was measured to assess respiratory motion.

Results: Target motion due to cardiac contraction was most prominent in the medial-lateral direction and of 4–5 mm magnitude. CTV_{Right} displacements were smaller in participants with AF than healthy participants in

normal sinus rhythm. Nearby cardiac structures often moved with different magnitudes and motion trajectories. CTV_{Left} and/or CTV_{Right} were in direct contact with the esophagus in 73% of participants. Target motion due to respiration was most prominent in the superior–inferior direction and of 13–14 mm magnitude in both healthy and AF participants.

Conclusion: AF CR target motion and relative displacement was characterized. The combination of target motion magnitude and relative displacement to critical structures highlights the importance of personalizing motion compensation techniques for effective AF CR treatments.

Key words: *Cardiac radioablation, non-malignant, arrhythmias, motion management*

TH – External beam – photons – Motion management (intrafraction)

TH – External beam – photons – Development (new technology and techniques)

IM/TH – image segmentation – MRI

IM/TH – MRI in Radiation Therapy – MRI for treatment planning

INTRODUCTION

The initial clinical success of cardiac radioablation (CR), an emerging non-invasive treatment alternative for cardiac arrhythmias, has been illustrated within publications describing over 50 human treatments for ventricular tachycardia. Its clinical adoption for atrial fibrillation (AF), the most common sustained cardiac rhythm disorder, has not been as comparably successful; publications report only three human CR treatments with only one patient remaining in sustained sinus rhythm beyond 6 months[1,2]. CR for AF presents additional challenges not encountered in radiation therapy for routine oncology nor CR for ventricular tachycardia: AF patients may fluctuate between normal and arrhythmic states during treatment delivery, treatment targets exhibit complex cardio-respiratory target motion, the targets are geometrically very close to critical structures and the wall of the atria is thin compared to other CR or radiation oncology treatment targets. Moreover, there is a higher risk that the patient could receive no therapeutic benefit yet suffer from radiation-induced CR toxicity.

The underlying electrophysiology of paroxysmal AF is multi-factorial but often includes disrupting electrical triggers originating within pulmonary vein (PV) musculature[3]. Catheter ablation, currently the gold-standard curative-intent non-pharmacological treatment, often electrically isolates the left atria (LA) from these disrupting electrical triggers by creating circumferential lesions around the PV ostia[3]. CR, which will now be referred to within the specific context of CR for paroxysmal AF, aims to non-invasively induce myocardial injuries analogous to those produced in catheter ablation using radiation therapy equipment and techniques. Prolonged treatment success will likely require complete circumferential transmural scarring that does not allow reconnection of abnormal electrical pathways. CR for AF will therefore need very accurate delivery of radiation treatments to small and mobile treatment targets to ensure full circumferential dose deposition is achieved while sparing surrounding critical structures.

The reported magnitude of cardio-respiratory displacement of cardiac structures has been variable and there is currently little consensus regarding optimal motion management techniques for CR. Cardiac-induced LA or PV displacement has been reported in the range 1–12 mm and cardiac structures even in close proximity have been shown to move with different magnitudes and motion trajectories[4-9]. Human studies specifically investigating CR target motion have either used healthy[4,7] or AF[8] participants, but no study has utilized the same methodology on both healthy and AF participants. Internal target volumes (ITVs) have been used to compensate for cardiac-induced target motion in animal studies[10-13], but human CR treatments[1,2] to date have not explicitly discussed any cardiac motion compensation. Respiratory-induced LA or PV displacement has been reported in the range 5–17 mm[4,5,8,14-16]. Animal and human CR treatments have utilized real-time x-ray imaging based fiducial or temporary lead tip tracking[11,17,18], ITVs[12,13], and breath-holds[10] for respiratory motion management. In-vivo dosimetry has scarcely been performed but measured target doses in animal CR treatments utilizing x-ray based fiducial tracking were on average 5–6% lower than planned[17] and delivered doses to the target volume in phantom studies utilizing combined cardio-respiratory multi-leaf collimator (MLC) tracking were on average 8% lower than

planned[5]. Lower target dose deposition may be due to limitations in motion management techniques and could compromise treatment efficacy.

The purpose of this study was to perform extensive motion characterization of the specific CR treatment target in both healthy and AF participants using magnetic resonance imaging (MRI) to help advise suitable CR motion management techniques and provide insight regarding optimal CR treatment planning and treatment delivery techniques.

MATERIALS AND METHODS

Figure 1 summarizes the methodology used in this motion characterization study utilizing MRI imaging.

Study participants

Ten healthy participants with no underlying cardiac conditions (5 males, mean age=42 years, standard deviation=14 years) and five participants diagnosed with AF (4 males, mean age=65 years, standard deviation=6 years) were recruited into this imaging study, which was approved by the New Zealand Health and Disability Ethics Committee. All participants provided informed consent prior to their inclusion and the study conformed to Good Clinical Practice standards.

AF participants exhibited symptomatic, drug refractory, paroxysmal or persistent AF, and were awaiting their first catheter ablation procedure as part of their clinical care. Four of the AF participants were in normal sinus rhythm for most of the image acquisition but exhibited a small number of short-lived arrhythmic episodes, ascertained via electrocardiography (ECG). One AF participant exhibited persistent AF throughout the imaging appointment. None of the healthy participants exhibited arrhythmias during image acquisitions.

Image acquisition

All study participants underwent non-contrast cardiac MRI image acquisition on a 3T Magnetom Skyra (Siemens, Germany) using an 18-channel body flex coil. ECG-gated, 2D cine images were acquired in end-expiratory breath-hold using a gradient echo fast low angle shot (FLASH) sequence. 8–16 contiguous slices were acquired in the transverse, coronal, and sagittal planes to encompass at least the LA and PV ostia. Retrospective ECG-gating was used in healthy participants to acquire 25–32 frames per cardiac cycle. An ECG-triggered acquisition was used for AF participants due to their varying heartrate and 18–28 frames per cardiac cycle were acquired, determined by the duration they were comfortably able to hold their breath. Un-gated cines were also acquired in free-breathing using a balanced stead-state coherent sequence (TrueFISP). 60–90 second acquisitions were acquired to capture combined respiratory and cardiac motion over multiple respiratory cycles. These single slice cines were acquired in the transverse, coronal, and sagittal planes sequentially, centered on either the left or right PV ostia. Further details regarding sequence parameters are provided in **Error! Reference source not found.**.

MRI sequence and parameter choice were determined from the results of an initial pilot study conducted by the authors of this study, which evaluated a variety of 1.5 T and 3 T MRI image pulse sequences for utilization within the clinical AF CR workflow on four human participants. Discussions with a cardiologist and radiation oncologist indicated that all attempted 3D acquisitions provided insufficient image quality for target delineation. The signal to noise ratio of the blood pool in or near the target region and the contrast to noise ratio (CNR) between the pulmonary veins near the target region and the surrounding lung tissue were significantly lower and the non-uniformity within the pulmonary veins were larger on 3D acquisitions compared to 2D acquisitions. The CNR within images acquired with cardiac-gated 2D TrueFISP and FLASH sequences were comparable but the variation of CNR throughout the cardiac cycle and non-uniformity was smaller in FLASH images. The TrueFISP images provided superior contrast between the myocardium and blood pool but were more prone to flow artefacts. No significant differences were seen between 1.5 T and 3 T image quality metrics.

Analysis

Motion due to cardiac contraction

To obtain 3D datasets, breath-hold ECG-gated cine stacks were interpolated into 1 mm voxel static images for each cardiac phase. The LA and CR treatment targets were manually delineated for every cardiac phase. Treatment targets will now be referred to as clinical target volumes (CTVs) to be aligned with radiation therapy terminology. In a clinical setting, this volume would be expanded with an additional margin to account for treatment uncertainties. Two CTVs were created for each participant; pair-wise circumferential disc volumes at the left (CTV_{Left}) or right (CTV_{Right}) pulmonary vein ostia. CTV_{Left} included the left superior and left inferior PV ostia and CTV_{Right} included the right superior and right inferior PV ostia, as shown in Figure 1b. CTVs closely resembled the wide-area circumferential ablation line commonly used in catheter ablation and were of approximately 3-4 mm width and full myocardial depth. Contouring was predominately performed on the dataset acquired in the transverse plane. The datasets acquired in the sagittal and coronal planes were registered to the transverse dataset and all contours were visually evaluated in all planes and modified as required. The 3D surface of the CTVs were qualitatively evaluated and modified as required to achieve continuity and smoothness.

Following the same contouring methodology as above, 3 mm diameter spherical regions-of-interest (ROIs) were contoured at the most antero-superior intersection of each PV with the LA and labelled: left inferior PV (LIPV), left superior PV (LSPV), right inferior PV (RIPV), and right superior PV (RSPV), as illustrated in Figure 1a. Care was taken to choose points that were of high contrast and in easily identified anatomical positions so that their 3D co-ordinate could be reliable identified in every image frame. All image interpolation and contouring were performed within MIM Maestro (MIM Software Inc, USA) by a single observer. Where available, radiation oncology contouring guidelines from the Radiation Therapy Oncology Group (RTOG) were followed[19-22].

The 3D co-ordinate location of the LA, CTVs and ROI centroids were determined for every cardiac phase and exported to MATLAB (Mathworks, USA). The maximum 3D displacement throughout the cardiac cycle was calculated. The maximum 2D displacement in the medial-lateral (ML), anterior-posterior (AP), and superior-inferior (SI) directions and the maximum relative displacement between CTV_{Left} and CTV_{Right} were also calculated. Centroid displacement throughout the cardiac cycle relative to LA end-systole (maximum filling) was evaluated in the ML, AP, and SI directions. Each participant's data were interpolated to 25 cardiac phases within MATLAB for inter-participant comparison.

The volume of the contoured LA was plotted as a function of image-frame to identify the frame that corresponded to LA end-diastole (maximum dilation) and end-systole. The 3D datasets for these two cardiac phases were identified and organs-at-risk (OAR) were contoured using the same methodology as target contouring. OARs included the esophagus, ascending aorta, descending aorta, spinal canal, closest vertebrae body, pulmonary arteries, superior vena cava, inferior vena cava and proximal bronchus. 3D contours were exported to MATLAB. The 3D Euclidean distance between every point on the CTV and OAR contour surfaces were calculated and the minimum Euclidean distance in n=3 dimensions was determined;

$$\text{minimum distance}_{target,OAR} = \min \sqrt{\sum_{i=1}^{n} (x_{itarget} - x_{iOAR})^2}.$$

Target proximity to surrounding structures was assessed for the 15 participants collectively as anatomical geometry was assumed to be independent of whether the participant had AF or not.

Target motion during free-breathing

2D cardio-respiratory target displacement was assessed on the 2D free-breathing cines. Circular ROI's of 3 mm diameter were contoured within or close to either the left or right CTV on every image frame. The free-breathing 2D cines were acquired in the plane of the most clearly visible pulmonary vein ostium and consequently this analysis did not differentiate between CTV_{Left} and CTV_{Right}.

To assess the suitability of other anatomical structures as motion surrogates, circular ROIs of 3 mm diameter were also contoured at the superior apex of the diaphragm dome and on the sternum at the sternal angle. Analysis of sternal motion was not performed on transverse images because the sternal angle could not be reliably identified and sternal motion in the LR direction was not analyzed as this was assumed to be negligible. The 2D co-ordinates of the ROI centroids for every image frame were exported to MATLAB and the maximum displacement was calculated. Linear regression plots and correlation analysis was also performed to evaluate the suitability of the diaphragm and sternum as motion surrogates.

Statistical analysis

Results of normally distributed data were reported as mean ± standard deviation. Comparisons of 3D displacements due to cardiac contraction between healthy and AF participants and 2D displacements due to respiration were performed with Mann-Whitney U tests. A p-value ≤ 0.05 was considered significant. For

multiple hypotheses testing, the false discovery rate was controlled using the Benjamini-Hochberg procedure with the false discovery rate set at 5%. Comparisons of 2D displacements between the CTVs and all other evaluated structures due to cardiac contraction were evaluated via the Kruskal-Wallis test. Subsequent multiple comparisons were performed with Dunn's test using a control column. A family-wise significance and confidence level of < 0.05 was used and the p values were multiplicity adjusted to account for multiple comparisons. To compare the respiratory motion of evaluated structures, simple linear regression analysis was performed, and a Pearson correlation coefficient was determined provided data were normally distributed, ascertained via the Shapiro-Wilk W test. The probability that the correlation occurred by chance was calculated and if the p-value was ≤ 0.05, the correlation was considered significant.

RESULTS

Cardiac contraction induced motion

The 3D and 2D cohort-averaged maximum displacements of evaluated structures due to cardiac contraction are displayed in Table 2. The cohort-averaged maximum 3D displacement over any two time-points within the cardiac cycle of CTV_{Left} and CTV_{Right} was 5.1±1.3 mm and 5.4±1.3 mm respectively in healthy participants and 4.2±1.5 mm and 3.7±0.5 mm respectively in AF participants. Of all the evaluated structures, the LA exhibited the largest 3D displacements and the RIPV exhibited the smallest 3D displacements in both healthy and AF participants. The 2D cohort-averaged maximum displacement of CTV_{Left} was largest in the ML direction in both healthy and AF participants (5.3±1.4 mm and 4.7±1.9 mm respectively). The 2D cohort-averaged maximum displacement of CTV_{Right} was largest in the AP direction in both healthy and AF participants (4.1±1.2 mm and 3.4±1.0 mm respectively). The 3D and 2D ML displacement of CTV_{Right} were significantly smaller in AF participants compared to healthy participants ($p=0.03$ and $p=0.04$ respectively).

Figure 2 displays the cohort-averaged motion trajectories of the evaluated structures throughout the cardiac cycle relative to end-systole. CTV_{Left} and CTV_{Right} displace laterally relative to each other throughout the cardiac cycle and this displacement was on average 6.5±2.1 mm and 4.0±2.7 mm larger at end-diastole compared to end-systole in healthy and AF participants respectively. Two AF participants had very little (<1.5 mm) relative CTV displacement in the ML direction. CTV_{Left} and CTV_{Right} moved anteriorly with LA dilation and exhibited only small SI motion.

The statistical significance of target (CTV_{Left} and CTV_{Right}) 2D maximum displacements due to cardiac contraction compared to other analyzed structures for healthy and AF participants are shown in Table 2. The 2D displacements of CTV_{Left} and CTV_{Right} were significantly different in the ML and AP directions in healthy participants. In healthy participants, no structure had comparable displacement to both CTV_{Left} and CTV_{Right} in all three directions. In healthy participants CTV_{Left} had comparable displacement to the LIPV, LSPV, and RIPV in all directions and the LA in the ML and AP directions and CTV_{Right} had comparable

displacement to the LSPV and RSPV in all directions. In healthy participants both CTV_{Left} and CTV_{Right} had comparable displacements to all evaluated structures except the LA in the SI direction. In AF participants, all evaluated structures had comparable displacement in all directions except CTV_{Left} and the RSPV in the AP direction.

Target proximity to surrounding structures

Figure 3 displays the 3D minimum Euclidean distance between the CTVs and surrounding structures. The cohort-averaged minimum distance between CTV_{Left} and the bronchial tree, descending aorta, esophagus and pulmonary arteries were all <10 mm. On average CTV_{Left} was closest to the descending aorta (2.6±1.4 mm and 2.3±1.9 mm for end-systole and end-diastole states respectively) but CTV_{Left} was in direct contact with the esophagus in six participants and the bronchial airways in two participants. The cohort-averaged minimum distance between CTV_{Right} and the esophagus, bronchial tree, inferior vena cava, pulmonary arteries, right atria, superior vena cava and vertebral body were <10 mm. CTV_{Right} was in direct contact with the esophagus in six participants, the superior vena cava in five participants and the pulmonary arteries in seven participants. The esophagus was in direct contact with either CTV_{Left} or CTV_{Right} in 73% of participants.

Target motion with free-breathing

Cohort-averaged maximum 2D displacements of the CTV, diaphragm and sternum in the free-breathing images are shown in Table 4. CTV and diaphragm displacements were largest in the SI direction. Displacement in this direction had the largest variability between participants. CTV and diaphragm ML and AP displacements were of comparable magnitude to the cardiac-induced ML and AP displacements seen earlier in Table 2. CTV SI displacements were smaller than diaphragm SI displacements and larger than sternal SI displacements in both healthy ($p<0.001$ and $p<0.001$ respectively) and AF participants ($p=0.004$ and $p=0.001$ respectively). There were no significant differences between displacements in healthy and AF participants.

There was strong and significant correlation between the CTV and diaphragm motion in the SI direction in all healthy and AF participants ($r=0.9\pm0.09$, $p\leq0.001$ and $r=0.9\pm0.06$, $p\leq0.001$ respectively). However, the magnitude of their displacements differed, and this difference varied between participants, as illustrated in Figure 4. Linear regression indicated that CTV SI displacement was on average 50% smaller than diaphragm SI motion with the range of 29–100% seen in the study participants. In both healthy and AF participants, CTV and diaphragm displacement in the AP direction were only very weakly correlated ($r=0.2\pm0.3$ and $r=0.4\pm0.4$ respectively), CTV and sternal displacement in the SI direction were weakly correlated ($r=0.4\pm0.2$ and $r=0.5\pm0.2$ respectively), and CTV SI and sternal AP displacements were correlated ($r=0.5\pm0.3$ and $r=0.6\pm0.3$ respectively). CTV and sternal correlations were stronger in participants with larger sternal displacement.

DISCUSSION

CR cardio-respiratory target motion was characterized using MRI in both healthy and AF participants. The results highlight the complexity of target motion and reinforces the importance of careful and appropriate selection of motion management techniques. Target (CTV_{Left} and CTV_{Right}) motion is complex: the two targets displace laterally relative to each other by 4–7 mm with LA dilation, cardiac structures in close proximity do not always move comparably, CTV_{Right} displacement appears to be smaller in AF participants compared to healthy participants and respiratory motion, which is most prominent in the SI direction, is comparable between healthy and AF participants. Despite human AF CR treatments to date not explicitly discussing or addressing cardiac motion management, the magnitude of target motion combined with the target proximity to critical structures suggests that cardiac motion management should be at least carefully evaluated to maximize treatment efficacy and direct respiratory motion management is essential.

Table 5 compares the cardiac-induced displacement results of this study to literature. Bahig *et al.* evaluated displacements at the PV-LA intersections in healthy participants using 4DCT[7] and reported comparable ML displacements and marginally smaller SI displacements than observed in this study. Constantinescu *et al.* analyzed cardiac-induced displacements of CR treatment targets in AF participants via 4DCT and reported comparable but marginally smaller displacements than this study but observed no dominating motion direction or motion patterns between participants[8]. Target and LA displacements observed in healthy participants within this study were larger than displacements reported by Ipsen *et al.* who evaluated LA and PV ostium displacement in healthy participants using MRI[4]. LA displacements observed in AF participants within this study were smaller than displacements reported by Patel *et al.* utilizing MRI to characterize LA motion in AF participants[6]. LA displacement in healthy and AF participants were comparable in this study, confusing the hypothesis that the variation seen in LA displacements in previous studies were due to different study participant cohorts. The cause of varying displacement magnitudes reported in literature for the same evaluated cardiac structure remains unclear and could be due to differences in analysis methodology, imaging modality, or participant variation within studies with small sample sizes.

3D cardiac-induced displacements observed in this study were largest in the LA and smallest in the RIPV and this is consistent with previous studies[4,6,7,14]. 2D cardiac-induced displacements were largest in the ML direction for most evaluated structures, which is aligned with some previous findings[6,7,9] and conflicting with others[8,23]. The relative lateral displacement of the left and right treatment targets has been observed with respiration but has not been extensively reported with cardiac contraction[24]. Previous studies reported large displacements in some participants, up to 16.9 mm[4,25], however these extremes were not observed in this study. Motion characterization of canine PVs[23] and porcine LA[26] indicate that displacement magnitudes in these studies are comparable to what is observed in human studies.

The differing displacement of cardiac structures even in close proximity to the targets observed in healthy participants in this study has also been reported in an MRI imaging study of AF patients[6]. In healthy participants, no single evaluated structure was always a suitable surrogate for both CTV_{Left} and CTV_{Right}. However, if target displacement and surrogacy accuracy is assessed for individual patients within the

clinical CR workflow then it is likely that appropriate surrogates will be found for each target. This reinforces the importance of evaluating the motion of the specific CR target when choosing suitable motion management techniques. AF participants in this study did not exhibit differing displacements between cardiac structures. This may be due to the small sample size or possibly altered cardiac haemodynamics and biomechanics in AF cohorts and these require further investigation.

The significant differences in CTV_{Right} and RIPV displacements between healthy and AF participants observed in this study requires further investigation in a larger cohort study, however the comparable displacements in all other evaluated structures suggests that most motion characterization and motion management verification data from studies utilizing healthy participants may be exchangeable to an AF cohort. Furthermore, the cardiac motions of the participant in persistent arrhythmia were indistinguishable to other AF participants and this participant had the largest displacement of right sided structures out of all the AF participants. The ability for motion management techniques to deal with fluctuating arrhythmic and normal sinus rhythm states during treatment delivery also does not appear as crucial as previously thought but requires further investigation.

Respiratory induced target displacements and patterns observed in this study were comparable to previous studies[4,8,15,16,25]. The range of respiration-induced motion in this and other studies is not surprising considering the inter- and intra- participant respiration variability. A previous study queried whether patients with cardiac comorbidities may have shallower and shorter respiratory periods[4], but this was not observed in this study. There have been mixed findings regarding whether the left and right PVs displace with differing magnitudes due to respiration but this was not assessed in this study[8,15,16]. Comparable to the results of this study, Ector *et al.* reported a strong correlation between the diaphragm and PV ostia with a ratio of PV and diaphragm motion ranging from 0.38–0.47 for different PVs, and a less pronounced correlation between the anterior sternal and PV displacements[15]. Constantinescu *et al.* reported correlation between the inferior displacement of the diaphragm and right PVs but not the left PVs[8]. The variation in diaphragm and target displacement with respiration observed in this study is therefore likely caused by a combination of inter-participant variation, 2D plane selection, as well variation in what PV was analyzed.

The proximity of the esophagus to the treatment targets and the variable anatomical positioning of the esophagus found in this study are in agreement with previous CR treatment planning study studies that reported direct contact or overlap between the esophagus and CR targets in 50–75% of participants[27,28]. Currently there is limited to no data regarding suitable dose constraints for intra-cardiac structures but a treatment planning study concluded that treatment target margin expansions of ≤3 mm are required to adequately spare surrounding extra-cardiac structures[14]. Target proximity to critical extra-cardiac structures combined with the magnitude of target cardio-respiratory displacement highlights the importance of careful patient selection, as CR may not be a feasible treatment option for a larger number of potential AF CR patients, as well as optimal motion management selection.

Conclusive recommendations regarding the necessity and accuracy requirements for AF CR motion management cannot be made without extensive *in-vivo* dosimetry data as well as further understanding of the required target dose and normal tissue toxicities of intra-cardiac structures. However, the findings of this study can advise potentially suitable motion management choices. A cardio-respiratory motion management technique would make CR treatments practically easier, however using different motion management strategies for cardiac-induced and respiratory-induced target motion is also feasible. The magnitude of respiratory-induced displacements combined with the target proximity to critical structures found in this study indicates that an ITV for cardio-respiratory motion management is not likely feasible for human AF CR treatments. The extent of cardiac-induced target motion and target proximity to critical structures observed in some patients indicates that an ITV for cardiac-induced target motion combined with an alternative respiratory motion management technique, such as breath-holds, respiratory-gating, x-ray based fiducial/ICD lead-tip/diaphragm respiratory tracking, may also be unsuitable if OAR dose constraints are exceeded. The lateral relative displacement of the left and right treatment targets with LA dilation suggests that if a tracking motion management technique is used, for example fiducial tracking or MLC tracking, then this may need to be applied for each target separately and the surrogacy accuracy of fiducials, catheter lead tips, and/or nearby structures needs to be very carefully evaluated. MRI-guided real-time motion management for the LA has been illustrated[4,14], however the differential LA and target displacement reported in this study requires further investigation for this technique. The concept of an ECG-gated and/or respiratory-gated treatment delivery appears feasible[29], however the suitability of this technique for arrhythmia patients with irregular ECG traces needs further investigation. The suitability and accuracy of respiratory-gating using an external surrogate placed on the sternum however requires further investigation due to only weak correlation between the sternum and target displacement. The diaphragm appears to be a well-suited surrogate for respiratory-induced target motion, however the differing magnitude between these two structures should be evaluated for the individual patient. The results of this study reinforce the importance of evaluating target motion and personalizing motion management techniques within the clinical CR workflow.

The findings of this study are limited by the small sample size, the small number of arrhythmia episodes during image acquisition within the AF cohort, and image acquisition limitations. Analysis on a larger number of AF participants would enable more conclusive CR motion management recommendations, particularly considering the large inter-patient variability of both arrhythmic states and target motion. While the AF participants did not have many AF episodes during image acquisition, all AF participants were awaiting catheter ablation for their AF clinical care and were therefore representative of the typical CR patient cohort. Cardiac motion was evaluated on 3D data-sets derived from multiple acquired 2D cardiac-gated images because the poor image quality of 3D MRI acquisitions would have correlated to significant target delineation difficulties and uncertainties. The methodology of creating 3D datasets from multiple 2D acquisitions is challenged by participant movement between 2D acquisitions and the limited spatial resolution perpendicular to the acquisition plane. The uncertainty caused by patient motion between 2D acquisitions was reduced by performing rigid image fusions and acquiring 2D cine stacks in three

orthogonal planes and interpolating datasets to 1mm voxel sizes helped reduce the uncertainty caused by the large MRI slice thickness. The reported displacements are limited by voxel size. Currently there is little consensus regarding optimal AF CR target contour definition so this study used treatment targets comparable to target lesions created during catheter ablation and targets used in animal and human AF CR treatments to date. Target delineation is limited by observer variability. The proximity of treatment targets to surrounding structures was analyzed only in end-expiration and some structures may move closer or further away with inspiration. Respiratory motion analysis could not be separated from cardio-respiratory motion within the free-breathing images and therefore respiratory-induced displacements were assessed by comparing the magnitude of cardio-respiratory induced displacements and cardiac-induced displacements. Nevertheless, this is the first study to evaluate cardiac and respiratory CR target motion, assess the surrogacy suitability of surrounding structures and target displacement to critical structures in both healthy and AF participants.

The MRI-based motion characteristic methodology used in this study could be incorporated within the clinical CR clinical workflow to characterize motion and personalize motion management techniques for the individual patient. 3D and/or 4DCT has been used in previous studies to characterize target motion but it has been reported that thorax tumor displacements can be incorrectly reported on CT acquisitions due to image artefacts, uncertainty in target delineations due to the limited soft tissue contrast, out-of-plane motion, and acquisition over only a small number of respiratory cycles[30]. Furthermore, CT requires ionizing radiation and the number of acquisitions or length of acquisitions needs to be conservative. MRI overcomes many of these challenges. However, commercially available 3D MRI acquisitions currently provide limited image quality around the left atria and pulmonary veins and this image modality is also known to suffer from geometric distortions and be prone to flow artefacts. This study has illustrated that 3D geometric information of sufficient image quality for target delineation can be obtained utilizing 2D MRI acquisitions for cardio-respiratory target motion characterization in both healthy participants with regular cardiac cycles and AF participants with irregular cardiac cycles. The heart was always positioned in the center of the field-of-view to keep geometric distortions <1 mm and MRI sequence optimization eliminated or significantly reduced flow artefacts. A pre-treatment MRI imaging appointment could also provide baseline images for consequent follow-up comparison or aid MRI-guided treatment deliveries.

CONCLUSION

The absolute and relative motion of CR for AF targets were characterized using MRI in both healthy and AF participants. The results demonstrate the complexity and variability of cardio-respiratory target motion. The combination of target motion magnitude and target proximity to critical structures highlights the importance of choosing suitable and optimal motion compensation techniques to ensure AF CR treatments are both effective and safe.

FIGURE CAPTIONS:

Figure 1: *Overview of study methodology (a) and exemplar 2D MRI images (b) acquired in a healthy participant with ECG-gating (left column) and an atrial fibrillation (AF) participant with ECG-triggering (right column) in the transverse (top row), coronal (middle row), and sagittal (bottom row) planes with exemplar target volumes (CTVs) contoured in red (online version).*

Figure 2*: Centroid displacements relative to cardiac phase 0% throughout the cardiac cycle are shown in the medial-lateral (top row), anterior-posterior (middle row) and superior-inferior (bottom row) directions for healthy (left) and atrial fibrillation (AF) (right) participants. The left target volume (CTV_{Left}) is shown in blue, the right target volume (CTV_{Right}) in green, and the left atria (LA) in orange solid lines. The left inferior pulmonary vein (LIPV) and left superior pulmonary vein (LSPV) are shown as blue dotted lines and the right inferior pulmonary vein (RIPV) and right superior pulmonary vein (RSPV) are shown in green dotted lines. Cardiac phase 0% represents end-systole and approximate 50% cardiac phase represents end-diastole. Cohort-averaged values are shown as solid symbols and error bars represent the standard deviation. For visual clarity, error bars are only displayed for CTV_{Left}, CTV_{Right}, and LA. An exemplar 3D segmentation is shown (middle) to indicate the direction of motion (CTV_{Left} in blue, CTV_{Right} in green, LA in orange).*

Figure 3: *Box-plots (box=inter-quartile range, box central line=median, whiskers=minimum and maximum values excluding outliers) of the minimum 3D Euclidean distance between the surface of CTV_{Left} contour and the surface of the surrounding structure contour (orange) and the minimum 3D Euclidean distance between the surface of CTV_{Right} contour and the surface of the surrounding structure contour (blue) in both end-systole (darker shade) and end-diastole (lighter shade) (online version).*

Figure 4: *Linear regression analysis comparing target (CTV) and diaphragm displacement in the superior-inferior (SI) direction for the five atrial fibrillation (AF) participants (left). The Pearson correlation coefficients r values are shown as well as the best-fit linear trend lines and a direct linear relationship line shown in a grey dotted line. 20 seconds of the five AF participants motion trajectories are also shown (right), derived from sagittal free-breathing images. The CTV is in red and the diaphragm is in blue (online version). Only the AF participants are shown as exemplar data for visual clarity of the figure. CTV and diaphragm SI displacement are very well correlated, however the magnitude of the displacement of the two structures was often different and this difference varied between participants, as illustrated by the different gradients in the linear trend-lines and in the motion trajectories.*

REFERENCES

1. Monroy E, Azpiri J, De La Pena C, et al. Late Gadolinium Enhancement Cardiac Magnetic Resonance Imaging Post-robotic Radiosurgical Pulmonary Vein Isolation (RRPVI): First Case in the World. *Cureus.* 2016;8(8):e738 doi:10.7759/cureus.738
2. Qian PC, Azpiri JR, Assad J, et al. Noninvasive stereotactic radioablation for the treatment of atrial fibrillation: First-in-man experience. *Journal of Arrhythmia.* 2020;36(1):67-74 doi:doi.org/10.1002/joa3.12283

3. Calkins H, Hindricks G, Cappato R, et al. HRS/EHRA/ECAS/APHRS/SOLAECE expert consensus statement on catheter and surgical ablation of atrial fibrillation. *Heart Rhythm.* 2017;14(10):e275-444 doi:10.1016/j.hrthm.2017.05.012

4. Ipsen S, Blanck O, Lowther N, et al. Towards real-time MRI-guided 3D localization of deforming targets for non-invasive cardiac radiosurgery. *Phys Med Biol.* 2016;61(22):7848 doi:10.1088/0031-9155/61/22/7848

5. Lydiard S, Caillet V, Ipsen S, et al. Investigating multi-leaf collimator tracking in stereotactic arrhythmic radioablation (STAR) treatments for atrial fibrillation. *Phy Med Biol.* 2018;63(18):195008 doi:10.1088/1361-6560/aadf7c

6. Patel AR, Fatemi O, Norton PT, et al. Cardiac cycle-dependent left atrial dynamics: implications for catheter ablation of atrial fibrillation. *Heart Rhythm.* 2008;5(6):787-793 doi:10.1016/j.hrthm.2008.03.003

7. Bahig H, de Guise J, Vu T, et al. Analysis of Pulmonary Vein Antrums Motion with Cardiac Contraction Using Dual-Source Computed Tomography. *Cureus.* 2016;8(7):e712 doi:10.7759/cureus.712

8. Constantinescu A, Lehmann HI, Packer DL, Bert C, Durante M, Graeff C. Treatment Planning Studies in Patient Data With Scanned Carbon Ion Beams for Catheter-Free Ablation of Atrial Fibrillation. *J Cardiovasc Electrophysiol.* 2016;27(3):335-344 doi:10.1111/jce.12888

9. Lickfett D, Dickfeld T, Kato R, et al. Changes of pulmonary vein orifice size and location throughout the cardiac cycle: dynamic analysis using magnetic resonance cine imaging. *Cardiovasc Electrophysiol.* 2005;16(6):582-588 doi:10.1111/j.1540-8167.2005.40724.x

10. Lehmann HI, Graeff C, Simoniello P, et al. Feasibility Study on Cardiac Arrhythmia Ablation Using High-Energy Heavy Ion Beams. *Sci Rep.* 2016;6:38895 doi:10.1038/srep38895

11. Sharma A, Wong D, Weidlich GA, et al. Noninvasive stereotactic radiosurgery (CyberHeart) for creation of ablation lesions in the atrium. *Heart Rhythm.* 2019;7(6):802-810 doi:10.1016/j.hrthm.2010.02.010

12. Blanck O, Bode F, Gebhard M, et al. Dose-escalation study for cardiac radiosurgery in a porcine model. *Int J Radiat Oncol Biol Phys.* 2014;89(3):590-598 doi:10.1016/j.ijrobp.2014.02.036

13. Bode F, Blanck O, Gebhard M, et al. Pulmonary vein isolation by radiosurgery: implications for non-invasive treatment of atrial fibrillation. *Europace.* 2015;17(12):1868-1874 doi:10.1093/europace/euu406

14. Ipsen S, Blanck O, Oborn B, et al. Radiotherapy beyond cancer: target localization in real-time MRI and treatment planning for cardiac radiosurgery. *Med Phys.* 2014;41(12):120702 doi:10.1118/1.4901414

15. Ector J, De Buck S, Loeckx D, et al. Changes in left atrial anatomy due to respiration: impact on three-dimensional image integration during atrial fibrillation ablation. *J Cardiovasc Electrophysiol.* 2008;19(8):828-834 doi:10.1111/j.1540-8167.2008.01128.x

16. Klemm HU, Steven D, Johnsen C, et al. Catheter motion during atrial ablation due to the beating heart and respiration: impact on accuracy and spatial referencing in three-dimensional mapping. *Heart Rhythm.* 2007;4(5):587-592 doi:10.1016/j.hrthm.2007.01.016

17. Gardner EA, Sumanaweera T, Blanck O, et al. In vivo dose measurement using TLDs and MOSFET dosimeters for cardiac radiosurgery. *J Appl Clin Med Phys.* 2012;13(3):3745 doi:10.1120/jacmp.v13i3.3745.

18. Zei PC, Wong D, Gardner E, Fogarty T, Maguire P. Safety and efficacy of stereotactic radioablation targeting pulmonary vein tissues in an experimental model. *Heart Rhythm.* 2018;15(9):1420-1427 doi:10.1016/j.hrthm.2018.04.015

19. Kong FM, Ritter T, Quint D, et al. Consideration of dose limits for organs at risk of thoracic radiotherapy: atlas for lung, proximal bronchial tree, esophagus, spinal cord, ribs, and brachial plexus. *Int J Radiat Oncol Biol Phys.* 2011;81(5):1442-1457 doi:10.1016/j.ijrobp.2010.07.1977

20. Feng M, Moran J, Koelling T, et al. Development and validation of a heart atlas to study cardiac exposure to radiation following treatment for breast cancer. *Int J Radiat Oncol Biol Phys.* 2011;79(1):10-18 doi:10.1016/j.ijrobp.2009.10.058

21. Duane F, Aznar MC, Bartlett F, et al. A cardiac contouring atlas for radiotherapy. *Radiother Oncol.* 2017;122(3):416-422 doi:10.1016/j.radonc.2017.01.008

22. Jabbour SK, Hashem SA, Bosch W, et al. Upper abdominal normal organ contouring guidelines and atlas: a Radiation Therapy Oncology Group consensus. *Pract Radiat Oncol.* 2014;4(2):82-89 doi:110.1016/j.prro.2013.06.004

23. Rettmann ME, Holmes DR, 3rd, Johnson SB, Lehmann HI, Robb RA, Packer DL. Analysis of Left Atrial Respiratory and Cardiac Motion for Cardiac Ablation Therapy. *Proc SPIE Int Soc Opt Eng.* 2015;9415;94152L doi:10.1117/12.2081209

24. Noseworthy PA, Malchano ZJ, Ahmed J, Holmvang G, Ruskin JN, Reddy VY. The impact of respiration on left atrial and pulmonary venous anatomy: implications for image-guided intervention. *Heart Rhythm.* 2005;2(11):1173-1178 doi:10.1016/j.hrthm.2005.08.008

25. Roujol S, Anter E, Josephson ME, Nezafat R. Characterization of respiratory and cardiac motion from electro-anatomical mapping data for improved fusion of MRI to left ventricular electrograms. *PLoS One.* 2013;8(11):e78852 doi:10.1371/journal.pone.0078852

26. Hasnain A, Suzuki A, Wang S, et al. Quantitative assessment of cardiac motion using multiphase computed tomography imaging with application to cardiac ablation therapy. *Medical Imaging 2018:*

Image-Guided Procedures, Robotic Interventions, and Modeling. 2018;10576:105762F doi:10.1117/12.2295438

27. Blanck O, Ipsen S, Chan MK, et al. Treatment Planning Considerations for Robotic Guided Cardiac Radiosurgery for Atrial Fibrillation. *Cureus.* 2016;8(7):e705 doi:10.7759/cureus.705

28. Xia P, Kotecha R, Sharma N, et al. A Treatment Planning Study of Stereotactic Body Radiotherapy for Atrial Fibrillation. *Cureus.* 2016;8(7):e678 doi:10.7759/cureus.678

29. Poon J, Kohli K, Deyell MW, et al. Technical Note: Cardiac synchronized volumetric modulated arc therapy for stereotactic arrhythmia radioablation — Proof of principle. *Medical Physics.* 2020;47(8):3567-3572 doi:10.1002/mp.14237

30. Sawant A, Keall P, Pauly KB, et al. Investigating the Feasibility of Rapid MRI for Image-Guided Motion Management in Lung Cancer Radiotherapy. *BioMed Research International.* 2014;2014:485067 doi:10.1155/2014/485067

ACKNOWLEDGEMENTS:

The authors would like to thank MIM Maestro for use of a research license and the staff at the Center of Advanced MRI (CAMRI) for their help and support with MRI acquisition.

CONFLICT OF INTEREST:

No conflicts of interest to report.

FUNDING:

Project funding was obtained from the Auckland Academic Health Alliance (AAHA) collaboration fund. Dr. Paul Keall additionally acknowledges support of an Australian Government NHMRC Senior Principal Research Fellowship.

ETHICAL STATEMENT:

Consent was obtained from all study participants prior to their participation in the imaging study. The study was carried out in accordance with the principles outlined in the journal ethical policy and in accordance with local statutory requirements. Ethics approval was obtained from the New Zealand Health and Disability Ethics Committee (Reference number 17/NTB/223)

Table 1: Overview of MRI sequence parameters used in this study.

Parameter	Cardiac-gated for healthy participants	Cardiac-gated for AF participants	Real-time un-gated for all participants
Scan type	FLASH	FLASH	TrueFISP
Cardiac gating	ECG-gated retrospective binning	ECG-triggered	Continuous acquisition
Frames per slice	25 - 32	18 - 28	100 - 200
Respiratory state	Breath-hold	Breath-hold	Free-breathing
Echo time (TE)	2.65 ms	2.65 ms	2.5 – 2.7 ms
Repetition time (TR)	22 – 38 ms	26 – 37 ms	201 – 207 ms
Flip angle	10°	10°	10°
Slice thickness	5 mm	5 mm	5 mm – 6 mm
In-plane pixel dimension	1.4 – 2 mm x 1.4 – 2 mm	1.5 – 1.7 mm x 1.5 - 1.7 mm	1.5 – 2 mm x 1.5 – 2 mm
Temporal resolution	85 – 100 ms	85 – 270 ms	200 – 250 ms
Number of slices per imaging plane	8 – 16	8 – 16	1
Percent sampling	80	80	50

AF = atrial fibrillation, ECG = electrocardiogram, FLASH = gradient echo fast low angle shot sequence, TrueFISP = a balanced steady-state coherent sequence

*Table 2: Cohort-averaged maximum displacement of cardiac radioablation treatment targets, left atria, and pulmonary vein ROIs due to cardiac contraction. Statistically significance differences between 3D or 2D displacements of healthy and AF participants are indicated with a * symbol.*

Structure	Dimension & direction	Cohort-averaged maximum displacement throughout the cardiac cycle	
		Healthy participants (mm)	AF participants (mm)
CTV_{Left}	**3D**	**5.1 ± 1.3**	**4.2 ± 1.5**
	ML	5.3 ± 1.4	4.7 ± 1.9
	AP	3.1 ± 1.1	1.7 ± 0.3
	SI	3.6 ± 1.9	2.3 ± 0.7
CTV_{Right}	**3D**	**5.4 ± 1.3**	**3.7 ± 0.5***
	ML	3.3 ± 1.2	2.5 ± 0.6*
	AP	4.1 ± 1.2	3.4 ± 1.0
	SI	2.8 ± 1.0	2.5 ± 0.8
LA	**3D**	**6.3 ± 2.1**	**6.0 ± 2.3**
	ML	4.3 ± 1.8	5.2 ± 1.9
	AP	3.7 ± 1.4	3.0 ± 0.9
	SI	4.6 ± 1.5	2.9 ± 1.1
LIPV	**3D**	**5.5 ± 1.6**	**5.1 ± 4.0**
	ML	5.9 ± 2.3	5.0 ± 3.8
	AP	4.0 ± 1.9	2.4 ± 1.3
	SI	2.8 ± 1.0	2.0 ± 1.8
LSPV	**3D**	**4.6 ± 1.5**	**4.6 ± 1.2**
	ML	5.0 ± 2.1	4.5 ± 1.1
	AP	3.4 ± 0.9	3.1 ± 1.1
	SI	1.9 ± 1.8	2.3 ± 1.7
RIPV	**3D**	**2.7 ± 0.6**	**3.5 ± 0.9**
	ML	2.8 ± 0.8	3.7 ± 0.9
	AP	2.6 ± 0.5	3.2 ± 0.9*
	SI	1.6 ± 1.2	0.8 ± 0.7
RSPV	**3D**	**5.3 ± 1.3**	**4.7 ± 1.2**
	ML	4.1 ± 1.2	3.4 ± 0.9
	AP	5.7 ± 1.3	5.5 ± 1.2
	SI	2.0 ± 1.2	2.5 ± 1.8

** indicates that the magnitude of 3D displacement in healthy participants was significantly different to the magnitude of 3D displacement in participants with atrial fibrillation, assessed via the Mann-Whitney U test and significance threshold of <0.05. Due to multiple hypotheses testing, the false discovery rate was controlled using the Benjamini-Hochberg procedure with the false discovery rate set at 5%.*

AF= atrial fibrillation, AP = anterior-posterior, CTVLeft = left atrial fibrillation cardiac radioablation treatment target, CTVRight =right atrial fibrillation cardiac radioablation treatment target, LA = left atria, LIPV = anterio-superior intersection of the left inferior pulmonary vein and the left atria, LSPV = anterio-superior intersection of the left superior pulmonary vein and the left atria, ML = medial-lateral, RIPV = anterio-superior intersection of the right inferior pulmonary vein and the left atria, RSPV = anterio-superior intersection of the right superior pulmonary vein and the left atria, SI = superior-inferior

Table 3: Evaluation of the statistical significance of CTV_{Left} and CTV_{Right} 2D maximum displacements due to cardiac contraction in healthy and atrial fibrillation participants in the medial-lateral, anterior-posterior, and superior-inferior directions compared to all other evaluated structures. Statistical significance was evaluated via the Kruskal-Wallis test. Subsequent multiple comparisons were performed with Dunn's test where the mean rank of each structure was compared to the mean rank of the CTV being assessed as the control column. A family-wise significance and confidence level of <0.05 was used and the multiplicity adjusted p values are displayed in the table to account for multiple comparisons. Green indicates no statistical significance and red indicates statistical significance (online version).

Direction	Participants	Target	Structure						
			CTV_{Left}	CTV_{Right}	LA	LIPV	LSPV	RIPV	RSPV
Medial-lateral	Healthy	CTV_{Left}	-	p=0.0080	p>0.99	p>0.99	p=0.55	p=0.058	p=0.054
		CTV_{Right}	p=0.0080	-	p=0.011	p=0.049	p=0.77	p>0.99	p>0.99
	AF	CTV_{Left}*	-	p=0.25	p>0.99	p>0.99	p>0.99	p>0.99	p=0.85
		CTV_{Right}*	p=0.25	-	p=0.071	p=0.21	p=0.13	p>0.99	p>0.99
Anterior-Posterior	Healthy	CTV_{Left}	-	p=0.0071	p=0.071	p>0.99	p>0.99	p>0.99	p<0.001
		CTV_{Right}	p=0.0071	-	p>0.99	p=0.041	p=0.30	p=0.0065	p>0.99
	AF	CTV_{Left}	-	p>0.99	p=0.48	p>0.99	p>0.99	p=0.38	p=0.0028
		CTV_{Right}	p>0.99	-	p>0.99	p>0.99	p>0.99	p>0.99	p=0.14
Superior-Inferior	Healthy	CTV_{Left}	-	p>0.99	p=0.028	p>0.99	p>0.99	p>0.99	p>0.99
		CTV_{Right}	p>0.99	-	p=0.0013	p=0.89	p>0.99	p>0.99	p>0.99
	AF	CTV_{Left}*	-	p>0.99	p=0.28	p>0.99	p>0.99	p>0.99	p>0.99
		CTV_{Right}*	p>0.99	-	p>0.99	p>0.99	p>0.99	p>0.99	p>0.99

** indicates a non-significant result in the Kruskal-Wallis test. CTV_{Left} = left atrial fibrillation cardiac radioablation treatment target, CTV_{Right} = right atrial fibrillation cardiac radioablation treatment target, LA = left atria, LIPV = anterior-superior intersection of the left inferior pulmonary vein and the left atria, LSPV = anterior-superior intersection of the left superior pulmonary vein and the left atria, RIPV = anterior-superior intersection of the right inferior pulmonary vein and the left atria, RSPV = anterior-superior intersection of the right superior pulmonary vein and the left atria.*

GREYSCALE VERSION of same figure

Table 3: Evaluation of the statistical significance of CTV_{Left} and CTV_{Right} 2D maximum displacements due to cardiac contraction in healthy and atrial fibrillation participants in the medial-lateral, anterior-posterior, and superior-inferior directions compared to all other evaluated structures. Statistical significance was evaluated via the Kruskal-Wallis test. Subsequent multiple comparisons were performed with Dunn's test where the mean rank of each structure was compared to the mean rank of the CTV being assessed as the control column. A family-wise significance and confidence level of

<0.05 was used and the multiplicity adjusted p values are displayed in the table to account for multiple comparisons. Greyscale shade indicates statistical significance.

Direction	Participants	Target	Structure						
			CTV_{Left}	CTV_{Right}	LA	LIPV	LSPV	RIPV	RSPV
Medial-lateral	Healthy	CTV_{Left}	-	p=0.0080	p>0.99	p>0.99	p=0.55	p=0.058	p=0.054
		CTV_{Right}	p=0.0080	-	p=0.011	p=0.049	p=0.77	p>0.99	p>0.99
	AF	CTV_{Left}*	-	p=0.25	p>0.99	p>0.99	p>0.99	p>0.99	p=0.85
		CTV_{Right}*	p=0.25	-	p=0.071	p=0.21	p=0.13	p>0.99	p>0.99
Anterior-Posterior	Healthy	CTV_{Left}	-	p=0.0071	p=0.071	p>0.99	p>0.99	p>0.99	p<0.001
		CTV_{Right}	p=0.0071	-	p>0.99	p=0.041	p=0.30	p=0.0065	p>0.99
	AF	CTV_{Left}	-	p>0.99	p=0.48	p>0.99	p>0.99	p=0.38	p=0.0028
		CTV_{Right}	p>0.99	-	p>0.99	p>0.99	p>0.99	p>0.99	p=0.14
Superior-Inferior	Healthy	CTV_{Left}	-	p>0.99	p=0.028	p>0.99	p>0.99	p>0.99	p>0.99
		CTV_{Right}	p>0.99	-	p=0.0013	p=0.89	p>0.99	p>0.99	p>0.99
	AF	CTV_{Left}*	-	p>0.99	p=0.28	p>0.99	p>0.99	p>0.99	p>0.99
		CTV_{Right}*	p>0.99	-	p>0.99	p>0.99	p>0.99	p>0.99	p>0.99

** indicates a non-significant result in the Kruskal-Wallis test. CTV_{Left} = left atrial fibrillation cardiac radioablation treatment target, CTV_{Right} = right atrial fibrillation cardiac radioablation treatment target, LA = left atria, LIPV = anterior-superior intersection of the left inferior pulmonary vein and the left atria, LSPV = anterior-superior intersection of the left superior pulmonary vein and the left atria, RIPV = anterior-superior intersection of the right inferior pulmonary vein and the left atria, RSPV = anterior-superior intersection of the right superior pulmonary vein and the left atria.*

Table 4: 2D displacement of the target (CTV), diaphragm and sternum on free-breathing images for both healthy and atrial fibrillation (AF) patients in the medial-lateral (ML), anterior-posterior (AP), and superior-inferior (SI) directions.

Structure	Direction	Displacement (mm)	
		Healthy participants	AF participants
CTV	ML	6.2 ± 2.2	8.1 ± 5.0
	AP	5.2 ± 4.0	5.7 ± 1.3
	SI	12.6 ± 2.0	13.9 ± 4.1
Diaphragm	ML	4.5 ± 1.3	9.1 ± 3.0
	AP	4.8 ± 4.6	5.5 ± 1.7
	SI	21.2 ± 5.4	22.1 ± 6.4
Sternum	AP	4.1 ± 2.1	3.9 ± 1.4

SI	3.9 ± 2.1	3.3 ± 1.4

Table 5: Comparison of cohort-averaged cardiac displacement results with literature.

	Healthy participants		**Atrial fibrillation participants**	
	This study	Literature	This study	Literature
Left CR target or PV ostium	5.1 ± 1.3 mm	3.3 ± 1.2 mm Ipsen *et al.*[4]	4.2 ± 1.5 mm	4.4 ± 1.2 mm Constantinescu *et al.*[8]
Right CR target or PV ostium	5.4 ± 1.3 mm	3.0 ± 0.9 mm Ipsen *et a.l*[4]	3.7 ± 0.5 mm	4.5 ± 1.4 mm Constantinescu *et al.*[8]
Left atria	6.3 ± 2.1 mm	3.9 ± 0.6 mm Ipsen *et al.*[4]	6.0 ± 2.3 mm	8.8 ± 2 mm Patel *et al.*[6]

CR = cardiac radioablation, PV = pulmonary vein.

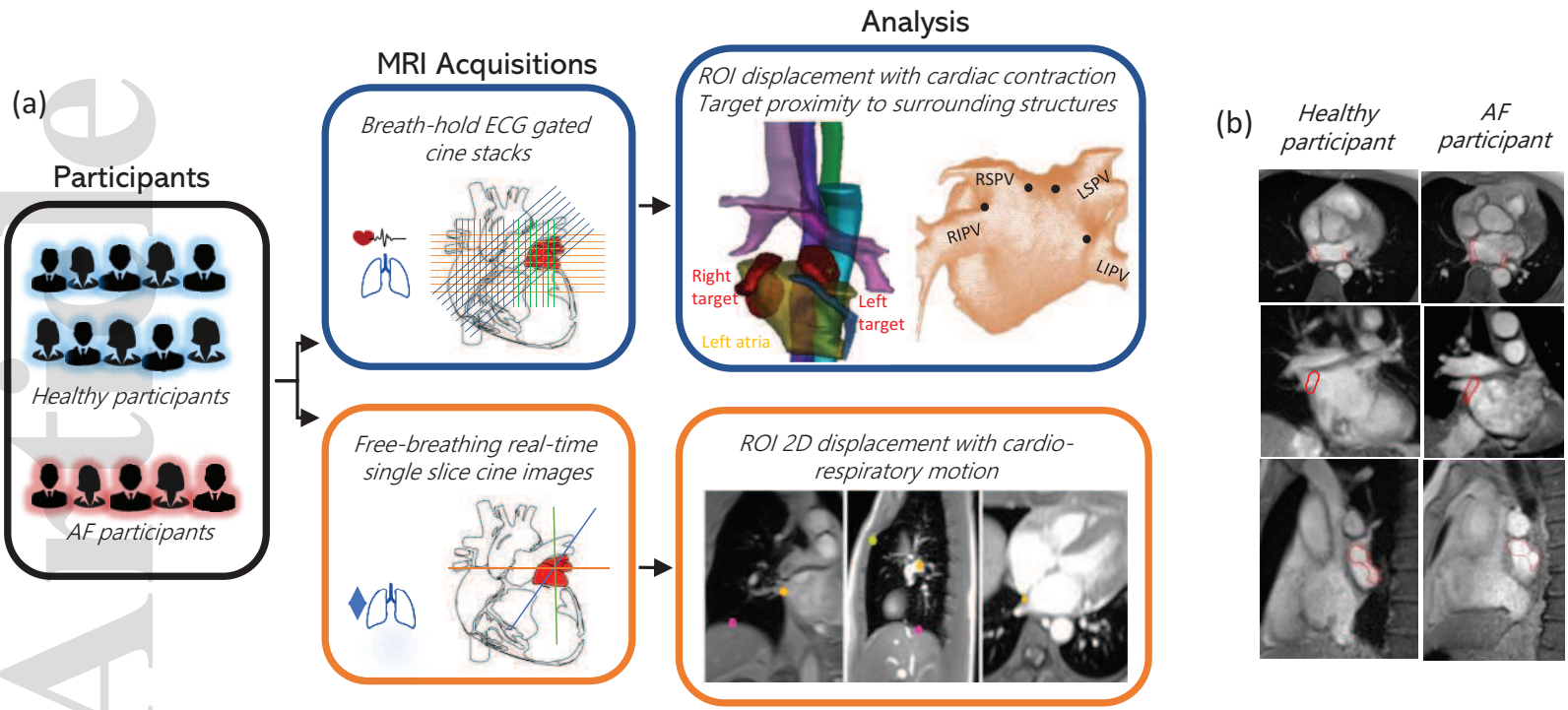

mp_14661_f1.eps

2D displacement of atrial fibrillation cardiac radioablation treatment targets and nearby cardiac structures throughout the cardiac cycle

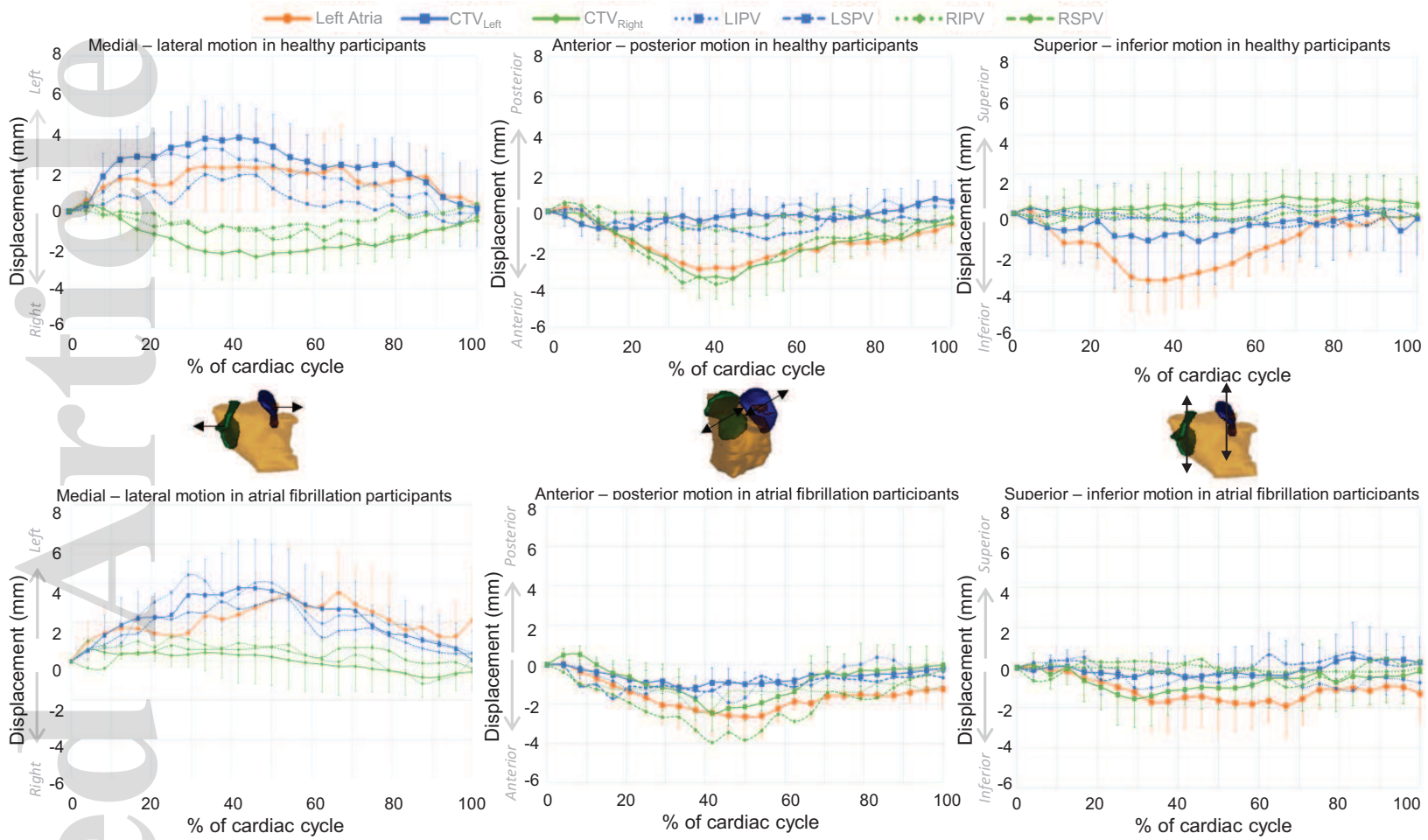

mp_14661_f2.eps

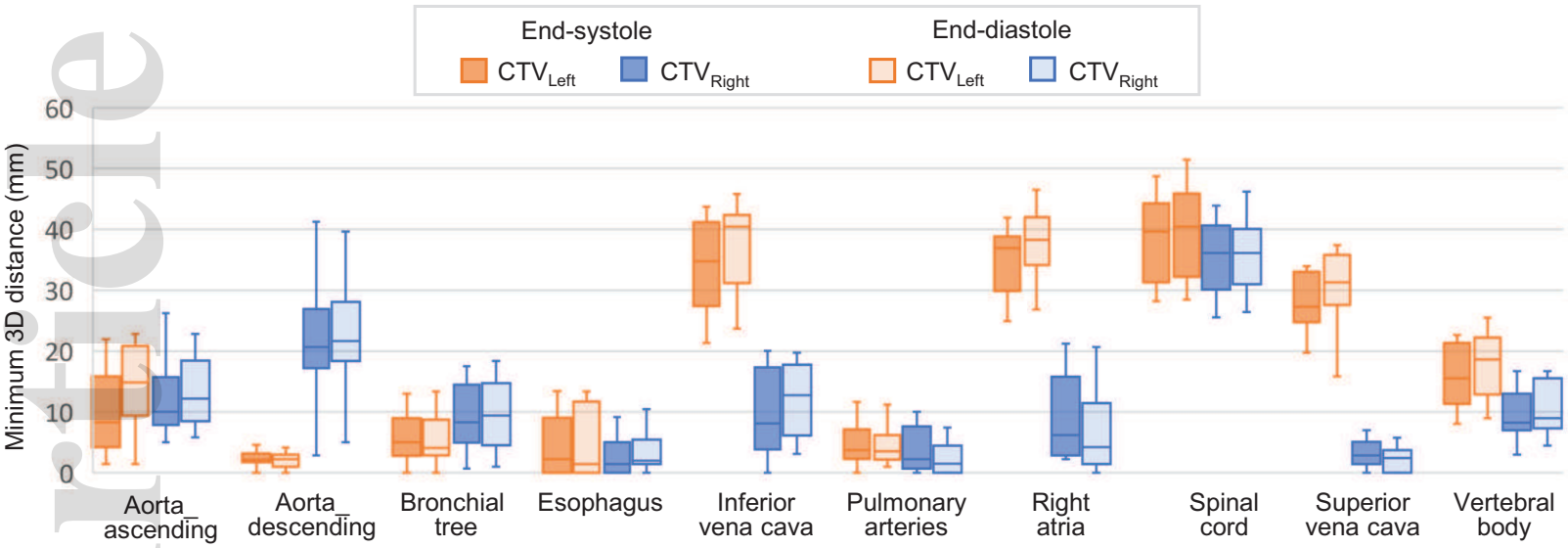

mp_14661_f3.eps

Comparison of target and diaphragm displacement in the superior-inferior direction in atrial fibrillation participants

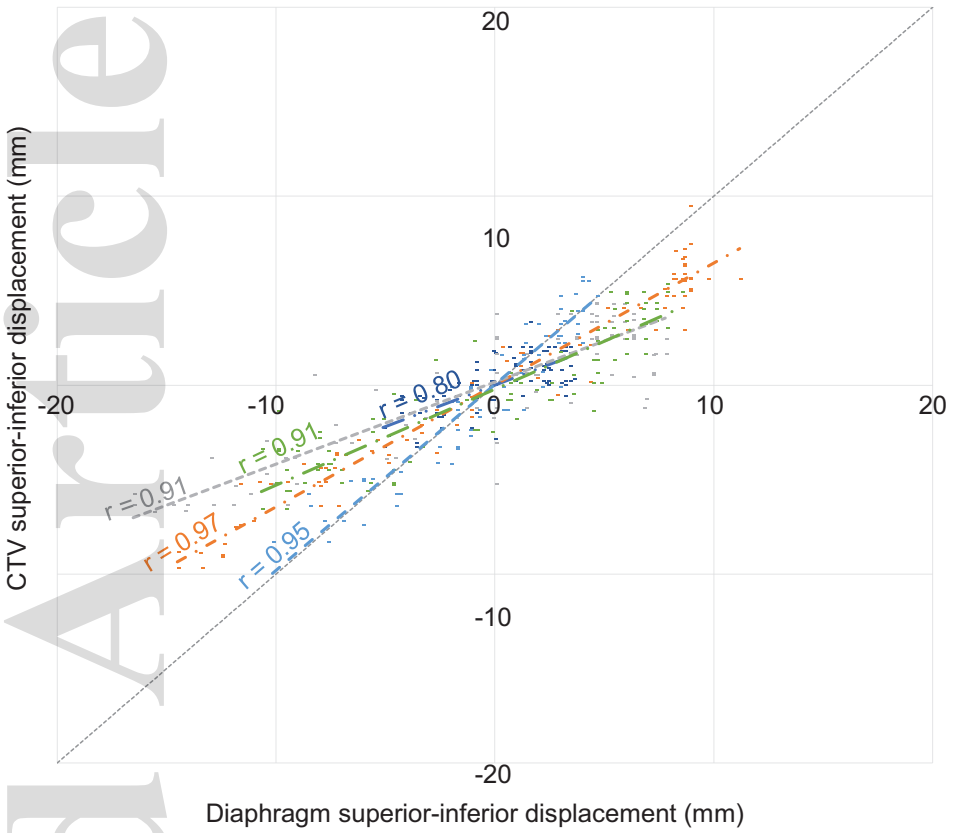

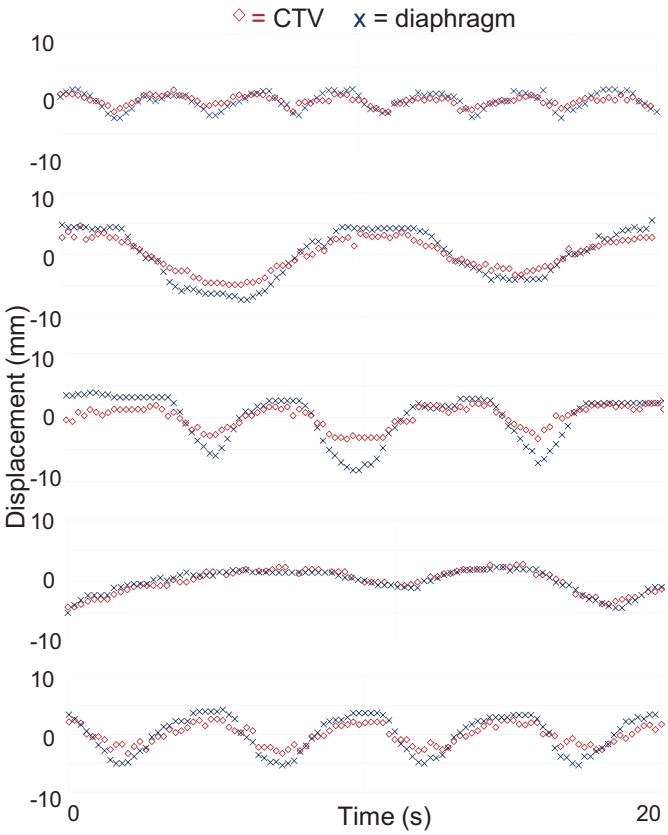

mp_14661_f4.eps